A Digital Pressure Sensor Based on Resonant Microbeams

D. W. Burns, J. D. Zook, R. D. Horning and W. R. Herb
Honeywell Technology Center
10701 Lyndale Ave S., Bloomington, Minnesota 55420

H. Guckel
University of Wisconsin Center for Applied Microelectronics
Madison, Wisconsin 53706

Abstract

A quasi-digital pressure sensor based on polysilicon resonant microbeams has been demonstrated. Pressure sensitivities of nearly 4,000 counts per second per psi have been attained on a 10-psi device with a base frequency of 233,000 Hz. The microbeams are fabricated with their own integral vacuum cavities, allowing high-Q operation in the differential pressure mode or in contact with liquids such as silicone oil. Design considerations include the effects of internal strain and lead to a push-pull layout configuration independent of microbeam strain or diaphragm thickness. Fabrication technology incorporates fine-grained polysilicon, surface micromachining, and reactive sealing. Packaging into precision avionics headers is being used for preliminary testing. Testing results indicate suitability for precision avionics, industrial, and commercial applications. Optical methods have been used to test resonant microbeam pressure sensors and verify the push-pull design methodology.

Introduction

Pressure sensors are second only to temperature sensors as the most important and widely used type of sensors being sold today. They are used to measure not only pressure but flow, fluid level, and acoustic intensities. More that ten different uses for pressure sensors have been identified in automotive applications. Honeywell introduced piezoresistive silicon sensors in the mid-1960s that, with continuous improvements, have been used extensively for precision pressure measurement in industrial controls and aircraft guidance controls. The trend in both of these areas is to increase the number of measurement points and the accuracy of the measurements under the premise that better information leads to better control.

Improvements in precision silicon micromachining technology during the past decade have led to a wide range of improved sensing structures, including the use of resonant microbeams as strain transducers.[1–7] With resonant sensors, the output is in the form of a robust sinusoidal signal whose frequency changes with pressure. The output is quasi-digital in the sense that it can easily be converted to digital form using a high frequency clock. Strain-sensitive mechanical-grade polysilicon resonators have been fabricated monolithically on silicon pressure diaphragms with integral vacuum-sealed cavities (see Figure 1) for differential or absolute pressure sensors that are usable in a wide range of applications.

Precision pressure applications now require "smart" transmitters that provide calibrated, temperature-compensated output in a specified format. Compensation for temperature and pressure nonlinearities requires calibration constants that must be stored in look-up tables and processing capability to execute the data correction algorithms. This capability is included in the package of a smart transmitter but not on the sensor chip. Use of a separate microcontroller chip that is interconnected to the sensor chip inside the package offers much greater flexibility and much faster time to market than combining them on the same chip. In this way, separate manufacturing processes can be used for each chip and there is no need to compromise the sensor or IC design or processing to achieve a merged process. In the case of the resonant sensors, it is possible to integrate the oscillator on the sensor chip using simple analog electronics. At the present time, however, we are using discrete surface-mount elements for the oscillator electronics.

Pressure Sensor Design

Static and dynamic structural modeling of the resonant microbeam and the sensor microstructure have been used extensively to guide the design of the resonant pressure sensor devices. Simplified analysis of a resonant microbeam pressure sensor requires a model of the deflection profile of the pressure diaphragm under load, the resulting applied strain to the microbeam(s) as a function of the position on the diaphragm, and the shift in resonant frequency of the microbeam with applied strain. With these basic elements, the microbeam frequency response as a function of applied pressure can be predicted as a function of geometry and material properties.

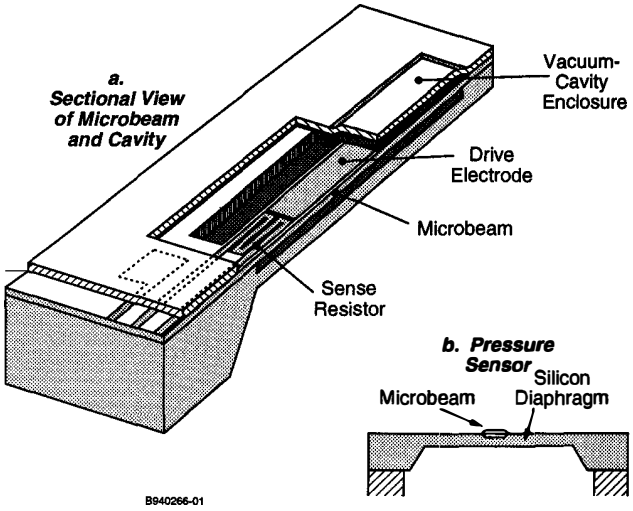


Figure 1. Cutaway view of a resonant microbeam. The sectional view in (a) shows the microbeam inside its vacuum-cavity enclosure with a central drive electrode and a position sensing microbeam at one end. A small ac voltage applied to the drive electrode electrostatically excites the microbeam, which is maintained by external drive/sense electronics. The resonant frequency of the microbeam shifts with applied axial strain. Selective positioning on a silicon diaphragm provides a large shift in frequency with differential pressure applied across the diaphragm.

The response of a undamped resonant microbeam element is governed by the following differential equation,[1,6] which includes the effects of intrinsic and applied strain:

$$EI\partial^4 w/\partial x^4 - (\varepsilon_O + \varepsilon_{app})EA\partial^2 w/\partial x^2 = -\rho A\partial^2 w/\partial t^2 \quad (1)$$

where w(x,t) is the lateral, time-dependent displacement of the beam along its length, E is Young's modulus of the beam material, I is the moment of inertia, ε_o is the internal or residual strain, ε_{app} is the applied strain to the beam ends, A is the beam cross-sectional area, and ρ is the mass density. This equation does not yield exact solutions, but approximate solutions can be found using energy or Rayleigh methods, which give the resonant frequencies of the beam. The resonant frequencies of a rectangular beam element of length l_b and thickness h_b are then given by Eq. 2 for doubly supported beams (clamped–clamped) and Eq. 3 for cantilever beams:

$$f_r = (b_n/2p)(E/\rho)^{1/2}(h_b/l_b^2)(1+\gamma_n(l_b/h_b)^2(\varepsilon_o+\varepsilon_{app}))^{1/2} \quad (2)$$

$$f_r = (c_n/2p)(E/\rho)^{1/2}(h_b/l_b^2) \quad (3)$$

The coefficients for the fundamental frequency and the first two overtones are summarized in Table 1.

0-9640024-0-X/hh1994/$20©1994TRF
DOI 10.31438/trf.hh1994.50

Table 1. Coefficients of resonant microbeams.

	b_n Doubly Supported	γ_n Doubly Supported	c_n Cantilever
Fundamental	6.4586	0.2949	1.0150
First Overtone	17.8034	0.1453	6.3608
Second Overtone	34.9018	0.08119	17.8104

To determine the applied strain to the microbeam, a model of the pressure sensor microstructure is required. With the pressure diaphragm in the form of a thin circular plate, the displacement profile under uniform applied pressure may be found in standard references[8] as:

$$w(r) = 3p_{app}(1-\upsilon^2)(a^2-r^2)^2/16Eh_d^3 \quad (4)$$

where w is the diaphragm deflection, p_{app} is the applied pressure, E and υ are Young's modulus and Poisson's ratio for the silicon diaphragm, a and h_d are the diaphragm radius and thickness, and r is the radial coordinate from the center. The corresponding strain distribution at the diaphragm surface is:

$$\varepsilon_r(r) = -(h_d/2)\partial^2 w/\partial r^2 = -3p_{app}a^2(1-\upsilon^2)(1-(r/a)^2)/8Eh_d^3 \quad (5)$$

For a microbeam mounted to the surface of the diaphragm, the strain applied to the beam may be calculated as the average diaphragm strain over the beam length. Eq. 6 and 7 give this result for two specific cases. Eq. 6 gives the applied strain to a microbeam of length l_b with one end mounted at the diaphragm edge and extending inward, while Eq. 7 gives the result for a beam centered on the diaphragm:

$$\varepsilon_a = 3p_{app}a^2(1-\upsilon^2)[2-3(l_b/a)+(l_b/a)^2]/8Eh_d^2 \quad (6)$$

$$\varepsilon_a = -3p_{app}a^2(1-\upsilon^2)[1-(l_b/2a)^2]/8Eh_d^2 \quad (7)$$

By combining Eq. 6 and 7 with Eq. 2, the change in microbeam resonant frequency with applied pressure may be determined for a variety of sensor layouts. For a dual-beam sensor layout, the sign difference between Eq. 6 and 7 implies a push-pull configuration, where the center- and edge-mounted microbeams undergo opposite applied strain and frequency shift with applied pressure.

To optimize the push-pull pressure sensor configuration, a sensitivity factor was defined to quantify the beam frequency response as

$$s_f = \Delta f/f_o/\Delta p_{app} \quad (8)$$

where Δf is the total frequency shift with pressure, f_o is the base frequency, and Δp_{app} is the change in pressure. Eq. 6, 7, and 8 may be used to calculate the sensor pressure sensitivity as a function of the beam length to diaphragm radius ratio. Figure 2 plots s_f versus l_b/a for the edge and center microbeams, and the combined push-pull configuration with equal length edge and center beams, with an assumed intrinsic strain value of 300 microstrain. This factor is maximized in the push-pull configuration for an l_b/a ratio of 0.4, a result that is independent of the beam and diaphragm thickness. This design choice also results in equal length beams, which provides first-order cancellations of microbeam nonlinearity and temperature effects.

An alternative sensor configuration with a single active beam on the diaphragm and a reference beam mounted off the diaphragm was also studied. Referring again to Figure 2, a sensor with a single center-mounted beam would have an optimum l_b/a ratio of about 0.6, a somewhat longer beam length than the optimal push-pull configuration. Unlike the push-pull configuration, the optimal singly active center-mounted design length varies significantly with the microbeam intrinsic strain level.

The design analysis was used to select the microbeam length-to-diaphragm diameter ratios to optimize the nominal frequency sensitivity of the resonant pressure sensor. The specific pressure sensor ranges can then be attained by varying diaphragm thickness without changing the layouts. The overall device performance has many other influences, including the microbeam drive/sense configuration. The details of the microbeam design and layout are further influenced by processing considerations, drive/sense electronics and packaging. Interconnects to the microbeam drive and sense lines are configured to minimize parasitic resistances and capacitances. The piezoresistor length is optimized to maximize the change in resistance with beam deflection. The electrostatic drive electrode may be optimized to selectively excite the fundamental mode and discourage higher order modes. Processing constraints affect the design rules for the microbeam, affecting in turn the minimum beam length and width. Packaging effects such as mechanical and thermal hysteresis are reduced by isolation techniques and the push-pull configuration.

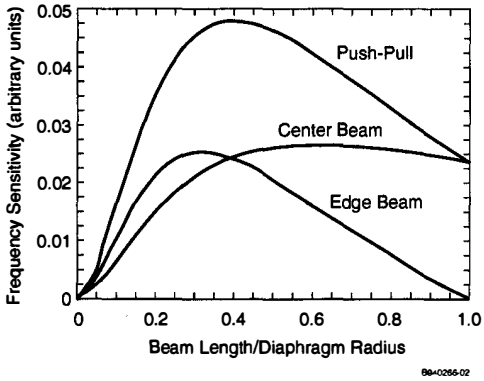


Figure 2. Pressure sensitivity of a resonant microbeam pressure sensor. The normalized shift in output frequency is plotted versus the microbeam length normalized to the diaphragm radius. The sensitivity of a center-mounted and an edge-mounted microbeam increases with length due to the increase in gage factor of the microbeam with increased aspect ratio (length/thickness) to a maximum value, then decreases due to a rapid reduction in the average applied strain. At the ratio $l_b/a = 0.4$, the frequency sensitivities of the two microbeams are equal in magnitude but opposite in sign, allowing subtraction and cancellation of first-order effects.

Sensor Fabrication

Resonant microbeam pressure sensors are fabricated on an n-type silicon epitaxial layer that is grown on a p-type substrate. The resonant microbeams are formed first, followed by diaphragm etching. Initial microbeam process steps include the growth and patterning of a thin oxide and deposited silicon nitride. Two local oxidations are done in the lower cavity region.[9] The first oxidation forms a depression in the silicon and is stripped off. The second oxidation deepens the depression to about 7500 Å and fills it in. The oxide forms a sacrificial layer upon which the beams are formed. The thin oxide film surrounding the depressions is patterned into narrow lines, forming channels for introduction of the sacrificial etchant later in the process. A 2-μm-thick film of mechanical-grade polysilicon, deposited over the oxide films and implanted, will form the resonant beam. The polysilicon piezoresistors are deposited and patterned over the beam poly. Following the piezoresistor formation, the beam poly is etched to define the exact beam dimensions, typically 46 μm wide × 200 μm long. A low-temperature oxide is then deposited and patterned to form a sacrificial layer above the beam. Another 2-μm-thick polysilicon film is deposited and patterned to form a shell over the beam and sacrificial layers. An HF solution penetrates through patterns etched in the shell and through the oxide channels. All oxide in the cavity is etched away, freeing the microbeams for vibration. After careful rinsing in water and cyclohexane baths, the wafers are placed in a vacuum chamber for sublimation of the solidified liquid in the shell. Following sublimation, the wafers are immediately placed in an LPCVD furnace to be evacuated and reactively sealed. Finally, contact openings are made to the substrate, piezoresistor, and shell, and PtSi contacts are formed in the openings. Aluminum is used for pads and for connection to the contacts. This completes the resonant microbeam formation, as shown in Figure 3.

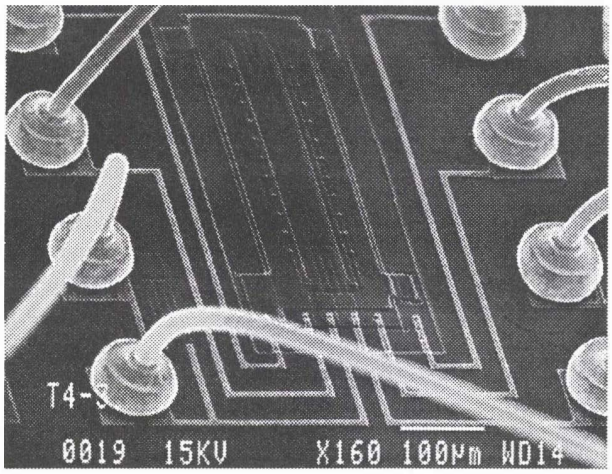


Figure 3. SEM of a wire-bonded resonant microbeam. Electrical interconnects are made to the drive line and sense lines of the 400-µm-long and 46-µm-wide microbeam.

An HF-based anodic etch is used to form the diaphragms. The backsides of the wafers are ground and polished to a thickness of about 280 µm. A Pt film is deposited and patterned with openings for the diaphragm etch. Additional pinhole protection is provided by a sputtered nitride film. The Pt acts as both the mask for the etching and as the contact to the p-type substrate. Etching is carried out in an HF-based electrolyte containing H_2SO_4 to allow higher current density.[10] The wafer is biased anodically at about 2–2.5 V with respect to a Pt counter electrode in the solution. The p-type substrate etches readily; etch stop occurs when the etch front reaches the n-type epilayer. This procedure forms a circular diaphragm with thickness determined by the initial epilayer thickness. Following removal of the backside nitride and Pt and the frontside protection layers, the wafer is diced and mounted in packages for testing.

Packaging and Test Results

Completed resonant microbeam pressure sensor wafers are probed optically to verify microbeam operation, frequency, and Q.[11] This noninvasive measuring technique requires the modulation of incident laser light around the microbeam resonant frequency. Reflected light is detected by a simple photodetector to locate microbeam resonances and determine Q.

Select die are electrically probed to verify drive line and piezoresistor impedances. The die are thermoelectrically bonded to a Pyrex tube, mounted in a Honeywell avionics product header, and wire bonded. A die with select microbeams wire bonded is shown in Figure 4. A metal lid can be welded on under vacuum to provide a vacuum reference for absolute pressure sensor measurements, or omitted for differential or gage pressure operation. The sensor die and header are mated with associated drive/sense electronics, as shown in Figure 5. The drive/sense electronics excite the microbeam into resonance and maintain it there as pressure is changed. The output is buffered for external data acquisition and analysis. The output frequency of a single microbeam as pressure is varied using a commercially available transfer standard is shown in Figure 6.

Linearity, span shift, null shift, and thermal hysteresis measurements are now under way on first units. Long-term testing on resonant microbeam devices have now exceeded 24,000 continuous operating hours without failure. Periodic checking of base frequency and Q shifts show little alterations. Continuous data taken on resonators suspended in a constant temperature bath show short-term stability as low as 0.01 ppm based on the fundamental resonant frequency. Frequency noise data for a typical microbeam is shown in Figure 7. The data represent nearly 100,000 measurement points. This device is being operated long term and has over 7,000 continuous operating hours.

Optical interrogation of the resonant microbeam pressure sensor has been demonstrated using the packaging and fixturing described above. Modulated incident laser light excites the microbeam into resonance. Resonances are detected by reflected light, as shown in Figure 8. Pressure applied to the backside of the diaphragm shifts the resonant frequencies of the microbeams to provide a measure of applied pressure, as shown in Figure 9. Optical testing shows high Q, high sensitivity, and excellent stability.

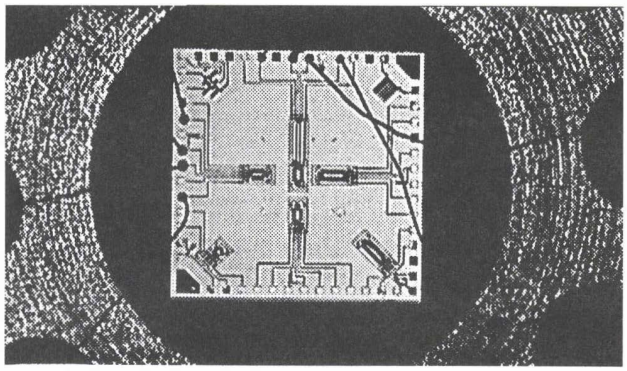


Figure 4. Resonant microbeam pressure sensor die. A multiplicity of resonant microbeams are located at the center and periphery of an isotropically etched silicon diaphragm and are selectively wire bonded for testing purposes. The die measures 3.3 mm × 3.3 mm.

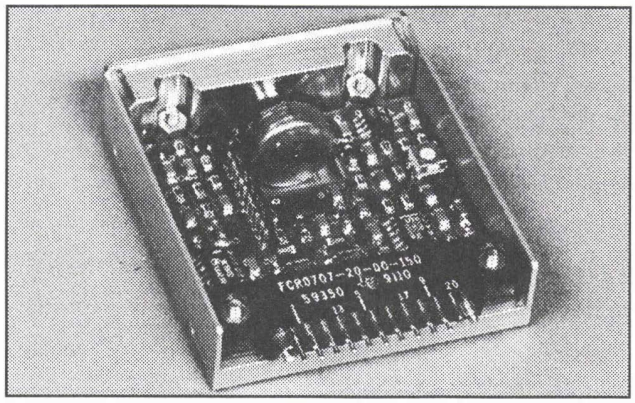


Figure 5. Packaged pressure sensor with digital output. The resonant microbeam pressure sensor die is located inside the circular metal can surrounded by the drive/sense electronics. The sensor is driven with standard ±12-V supplies and a buffered frequency output is available at one of the pins. The pressure port is located on the opposite side of the stainless steel manifold.

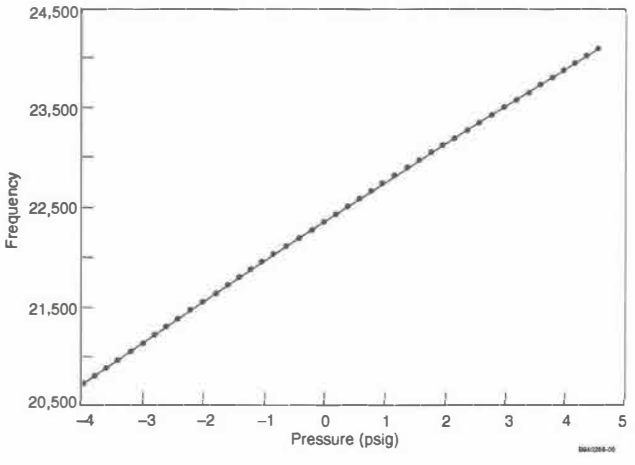


Figure 6. Frequency output in differential mode. Operating at a base frequency of 223,000 Hz, the pressure sensitivity is 3,880 Hz/psi.

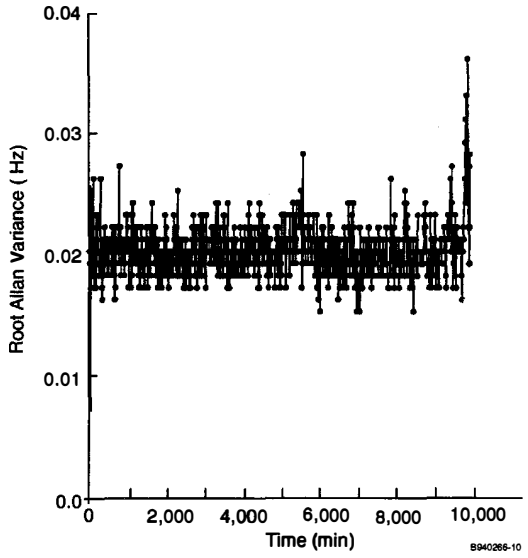


Figure 7. Root Allan variance of a resonant microbeam. This plot is a compilation of 100 consecutive paired variance data taken every 10 min over the time frame of a week, showing short-term stability of 0.02 Hz for a base frequency of 625,000 Hz.

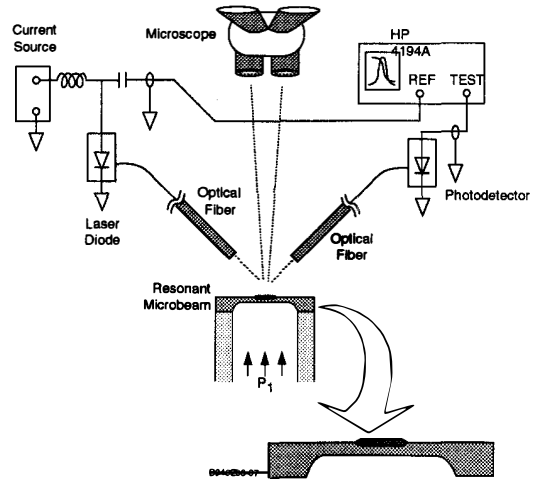


Figure 8. Optical test arrangement for resonant microbeam pressure sensor. An isotropically etched silicon die with polysilicon resonators is mounted on a Pyrex tube. Pressure applied up the tube creates bending stresses in the diaphragm that cause shifts in the resonant microbeam frequency. Excitation of the microbeam is achieved with modulated incident laser light and sensed with a simple photodetector.

Results and Conclusions

Resonant microbeam technology combines precision polysilicon microbeam strain sensors with conventional silicon microstructures to produce high-quality silicon sensors that integrate the digitizing function directly at the sensor. Interconnection with digital control systems is possible via electrical or optical means, allowing remote operation in harsh environments where immunity to EMI or intrinsic safety is required. The large gage factors of a resonant microbeam and its integral vacuum cavity to maintain high-Q operation allow large signals to be obtained with minimal strain for avionics and industrial applications such as differential pressure sensors.

Acknowledgments

The authors wish to acknowledge the Wright Laboratory Electronic Technology Directorate for partial funding of this activity. We would also like to acknowledge Jerry Huber and Bob Martin for sensor processing, Cindy Bassett for testing, and the Honeywell Solid State Electronics Center for providing precision packaging and wire bonding of the sensors.

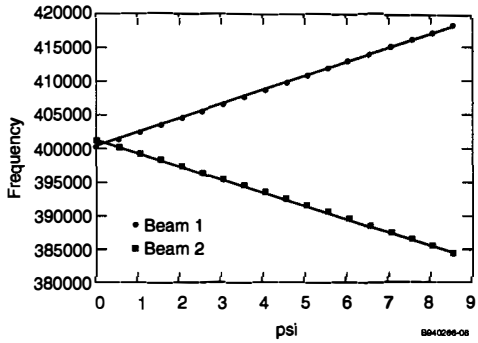


Figure 9. Output frequencies for the optical resonant microbeam pressure sensor. Two microbeams in the push-pull configuration are independently tested while pressure to the backside of the diaphragm is altered. The base frequencies of each microbeam is just over 400,000 Hz with a pressure sensitivity of nearly ±2,000 Hz/psi.

References

1. Sniegowski, J.J., "Design and Fabrication of the Polysilicon Resonating Beam Force Transducer," PhD Dissertation, University of Wisconsin–Madison, 1991.

2. Ikeda, K.; Kumayama, H.; Koboyashi, T.; Wanabe, T.; Nishikawa, T.; Yoshida, T; and Harada, K., "Silicon Pressure Sensor Integrates Resonant Strain Gauge on Diaphragm," *Sensors and Actuators,* A21–23 (1990), pp. 146–150.

3. Petersen, K.; Pourahmadi, F.; Brown, J.; Parsons, P.; Skinner, M.; and Tudor, J., "Resonant Beam Pressure Sensor Fabricated with Silicon Fusion Bonding," Transducers '91, *Proceedings of the 1991 IEEE Conference on Solid-State Sensors and Actuators,* San Francisco, June 24–28 1991, pp. 664–667.

4. Guckel, H.; Rypstat, C.; Nesnidal, M.; Zook, J.D.; Burns, D.W.; and Arch, D.K., "Polysilicon Resonant Microbeam Technology for High-Performance Sensor Applications," *IEEE Solid-State Sensor and Actuator Proceedings,* Hilton Head Is., SC, June 22–25, 1992, pp. 153–156.

5. Zook, J.D.; Burns, D.W.; Guckel, H.; Sniegowski, J.J.; Engelstad, R. L.; and Feng, Z., "Characteristics of Polysilicon Resonant Microbeams," *Sensors and Actuators,* A35 (1992), pp. 51–59.

6. Tilmans, H.A.C., "Micromechanical Sensors Using Encapsulated Built-in Resonant Strain Gauges," PhD Dissertation, University of Twente, Enschede, The Netherlands (1993).

7. Nikolich, A.D., and Senturia, S. D., "A Wafer-Bonded Silicon Load Cell Operating in the Tensioned-Wire Regime," *IEEE Solid-State Sensor and Actuator Proceedings,* Hilton Head Is., SC, June 22–25, 1992, pp. 157–160.

8. Timoshenko, S., *Theory of Plates and Shells,* 2nd edition, McGraw-Hill, 1959.

9. Sniegowski, J.J.; Guckel, H.; and Christensen, T.R., "Performance Characteristics of Second-Generation Polysilicon Resonating Beam Force Transducers," *IEEE Solid State Sensor and Actuator Workshop,* Hilton Head Is., SC, June 1990, pp. 9–12.

10. Wen, C.P., and Weller, K.P., *J. Electrochem. Soc.*, 119, 547, 1972.

11. Guckel, H.; Nesnidal, M.; Zook, J.D.; and Burns, D.W.; "Optical Drive/Sense for High-Q Resonant Microbeams," Transducers '93, *Proceedings of the 7th International Conference on Solid State Sensors and Actuators,* Yokohama, Japan, June 7–10 1993, pp. 686–689.